Bahraminasab *et al.*
BioMedical Engineering OnLine (2024) 23:127
https://doi.org/10.1186/s12938-024-01320-1

BioMedical Engineering OnLine

RESEARCH Open Access

Development of a hydrogel-based three-dimensional (3D) glioblastoma cell lines culture as a model system for CD73 inhibitor response study

Marjan Bahraminasab[1], Samira Asgharzade[2,3], Ali Doostmohamadi[4], Atefeh Satari[2,3], Farkhonde Hasannejad[4,5] and Samaneh Arab[1*]

*Correspondence:
Samaneh.arab@gmail.com

[1] Department of Tissue Engineering and Applied Cell Sciences, School of Medicine, Semnan University of Medical Sciences, Semnan, Iran
[2] Cellular and Molecular Research Center, Basic Health Sciences Institute, Shahrekord University of Medical Sciences, Shahrekord, Iran
[3] Department of Molecular Medicine, School of Advanced Technologies, Shahrekord University of Medical Sciences, Shahrekord, Iran
[4] Student Research Committee, Semnan University of Medical Sciences, Semnan, Iran
[5] Genetic Department, Breast Cancer Research Center, Moatamed Cancer Institute, ACECR, Tehran, Iran

Abstract

Background: Despite the development of various therapeutic approaches over the past decades, the treatment of glioblastoma multiforme (GBM) remains a major challenge. The extracellular adenosine-generating enzyme, CD73, is involved in the pathogenesis and progression of GBM, and targeting CD73 may represent a novel approach to treat this cancer. In this study, three-dimensional culture systems based on three hydrogel compositions were characterized and an optimal type was selected to simulate the GBM microenvironment. In addition, the effect of a CD73 inhibitor on GBM cell aggregates and spheroids was investigated as a potential therapeutic approach for this disease.

Methods: Rheology measurements, Fourier transform infrared spectroscopy (FT-IR), scanning electron microscopy (SEM) and cell proliferation assays were performed to analyze the synthesized hydrogel and select an optimal formulation. The viability of tumor cells in the optimal hydrogel was examined histologically and by confocal microscopy. In addition, the sensitivity of the tumor cells to the CD73 inhibitor was investigated using a cell proliferation assay and real-time PCR.

Results: The data showed that the hydrogel containing 5 wt% gelatin and 5 wt% sodium alginate had better rheological properties and higher cell viability. Therefore, it could provide a more suitable environment for GBM cells and better mimic the natural microenvironment. GBM cells treated with CD73 inhibitors significantly decreased the proliferation rate and expression of VEGF and HIF1-α in the optimal hydrogel.

Conclusion: Our current research demonstrates the great potential of CD73 inhibitor for clinical translation of cancer studies by analyzing the behavior and function of 3D tumor cells, and thus for more effective treatment protocols for GBM.

Keywords: Glioblastoma, Gelatin–alginate hydrogel, 3D cell culture, CD73 inhibitor

Introduction

Identifying novel treatments and predicting their response in cancer patients has remained a fundamental challenge in oncology [1, 2]. In brain tumors, surgical removal is often not possible and must be followed by radiation and chemotherapy. Most patients with glioblastoma multiforme (GBM), have a poor prognosis regardless of the treatment and die within 2 years of diagnosis [3–5].

CD73, an enzyme that generates extracellular adenosine, promotes cancer progression and protects tumors from immune response [6, 7]. Recent in vitro and animal studies have shown that CD73 may be a potential aid for the treatment of glioblastoma. Furthermore, CD73 promotes GBM angiogenesis [8]. Silencing of this molecule by siRNA or enzymatic inhibition has been shown to result in delayed tumor growth and improved survival in animal models of glioblastoma [9, 10]. Increased CD73 expression was observed in GBM tumor samples, and there was a closer association between NT5E overexpression and patient survival [11]. Glioma-derived CD73 contributes to local adenosine-mediated immunosuppression, and CD73 downregulation was a positive prognostic factor related to prolonged disease-free survival of glioblastoma patients [12]. In addition, CD73 is an ideal therapeutic target for cancer treatment especially in combination with conventional therapies and/or other immune checkpoint inhibitors [13]. The absence of CD73 in a murine model of glioblastoma treated with anti-CTLA-4 and anti-PD-1 prolonged survival [14].

The growth, metastasis and progression of tumors are largely dependent on the processes of angiogenesis and invasion [15]. VEGF is a potent endothelial survival factor that increases vascular permeability and acts as survival factor for endothelial cell. HIF-1α is a key factor in hypoxia and activates VEGF gene expression by binding to the HRE in the VEGF promoter region [16]. In addition to hypoxia and necrosis, GBM is characterized by advanced angiogenesis associated with overexpression of VEGF and HIF-1α. A very important factor in tumor invasion is the disruption of basement membrane integrity and active translocation of neoplastic cells by ECM matrix metalloproteinases (MMPs) such as the MMP9 gene, which is considered an important factor in ECM degradation and metastasis and has a positive correlation with brain tumor aggressiveness and MMP9 concentration [17].

Although various cell culture and animal studies have been used to evaluate the efficacy of anti-tumor agents, it remains difficult to predict patient response to treatment. Standard two-dimensional (2D) cell culture systems cannot accurately reproduce the tissue structures or the interactions between cells and their environment that regulate cell survival, development, apoptosis, migration, and drug resistance [18, 19]. The 2D cell culture systems are not representative the in vivo cell–cell and cell–ECM interactions. Therefore, they can result in deviation from in vivo responses [20–22]. Moreover, animal models of brain tumors and xenografts are difficult to use for large-scale drug sensitivity testing. To overcome these limitations, three-dimensional (3D) culture systems have been developed, in which a culture environment is provided allowing the embedded cells to grow and interact with the surrounding framework, as an extracellular matrix (ECM), in three dimensions. This cell culture approach is in contrast with traditional 2D cell cultures where the cells are

grown and form a flat monolayer at the plate surface. Therefore, 3D culture systems are more realistic compared to 2D cell culture, as the cells in human body are all in 3D environment. These systems are of particular importance in study of tumors, because the cell aggregates and spheroids formed in the framework act like a real tumor. Therefore, the 3D culture systems can mimic the in vivo tumor behavior and appears to be a powerful tool for identifying new therapies for brain tumors [23, 24].

To make the surrounding environment for tumor cells in 3D culture, different biomaterials have been employed. Among these materials, hydrogels are a unique group of hydrophilic polymers, which are increasingly being used for this purpose. Hydrogels have acceptable biocompatibility and similarity to the natural ECM, which promotes the influx of cell metabolites and enables cell growth, migration, and survival. Consequently, hydrogel-based matrices are convenient substitutes for in vitro 2D models [25]. The culture platforms provided by hydrogels are currently used in cancer research to test anti-cancer drugs for discovery, screening and dosage identification. The previous studies showed that the hydrogel systems better mimic the cell–cell and cell–matrix interactions that occur in innate tumor tissue, for example, by inducing cell aggregations and spheroid formation [26, 27].

Natural polymers are promising biomaterials for hydrogel synthesis due to their high biocompatibility and biodegradability. Hydrogels having sodium alginate (SA, a natural polysaccharide) in their compositions are attractive materials with cell encapsulation and drug delivery ability, which are widely used in 3D culture of cancer cells [28–30]. Cross-linking of alginate gels can be achieved by exchanging sodium ions with multivalent cations such as Ca^{2+}, e.g., by using $CaCl_2$ [31]. However, to form biomimetic hydrogel 3D structures with close similarity to the native ECM, protein components, in addition to polysaccharides, are also needed [25]. The main components of the brain ECM include the hyaluronan, chondroitin sulfate, lecticans, and tenascins [32]. These components belong to the family of polysaccharides and proteins in the form of glycosaminoglycans, proteoglycans and glycoproteins. In analogy with protein parts of brain ECM, gelatin (G) a denatured form of animal collagen derived from partially hydrolyzed collagen [33], can be used. Gelatin is a biocompatible, biodegradable, and cheap biomaterial with low antigenicity and high biodegradation rate, and it has found wide applications in tissue engineering and cell encapsulation [34–36]. The combination of sodium alginate and gelatin may be advantageous. The alginate hydrogels covalently cross-linked with gelatin have been shown to exhibit high cell adhesion, spreading, migration, and proliferation, as well as rapid degradation rates, which makes them suitable materials for cell encapsulation [37–39].

To the best of the authors' knowledge, the anti-tumor effect of CD73 inhibitor on glioblastoma animal and human cell lines has not been studied in a 3D culture model of gelatin–sodium alginate (G-SA) hydrogel. Therefore, three G-SA hydrogels with different concentrations of compounds were formulated and synthesized. To develop and evaluate a 3D culture system for brain tumors, human and rodent glioblastoma cell lines (U87 and C6, respectively) were individually used in hydrogels and the effect of CD73 inhibitor on their proliferation and expression of tumor-related genes was investigated.

Result

Characterization of the hydrogel scaffold

Chemical bonds

FTIR and ATR-FTIR analyses were used to identify the chemical functional group of the raw materials (i.e., gelatin and sodium alginate powders), and gelatin–sodium alginate hydrogels after cross-linking, for which the results are represented in Fig. 1. The SA spectra represented a subtle peak around 3430 cm^{-1}, as a consequence of the hydrogen-bonded OH group. The peaks that appeared at 1631 cm^{-1} and 1403 are due to the C=O of the carboxylate (COO^{-}) group of alginates. The bands between 1100 and 1000 cm^{-1} are due to the C–O–C groups. Similar peaks were observed in previous studies [40–42].

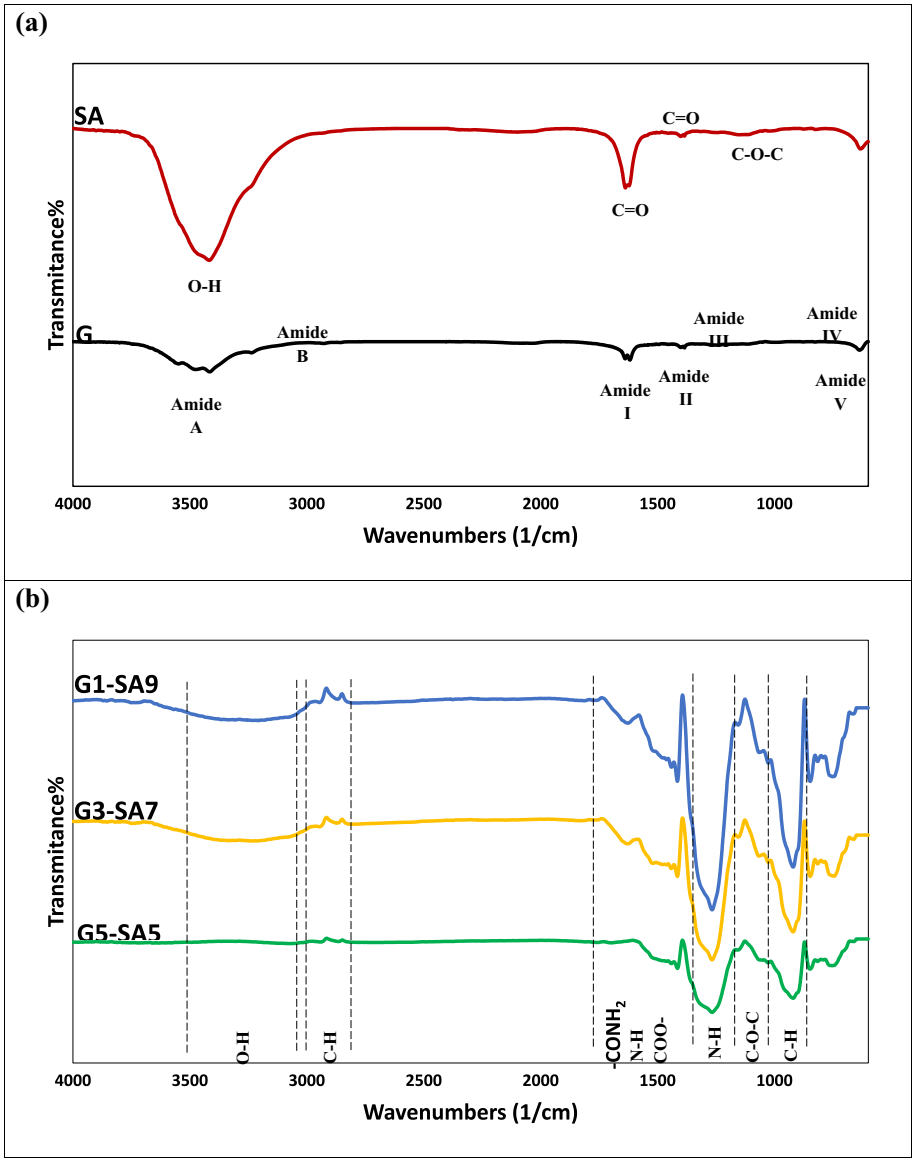

Fig. 1 Characterization of the hydrogels. FTIR spectra of **a** gelatin and sodium alginate powder, and **b** hydrogels

FTIR spectra of the gelatin are also shown in Fig. 1. In this spectrum, the characteristic peaks appeared between 1900 and 900 cm^{-1} (at about 1638 cm^{-1}, 1385 cm^{-1}, and 1256 cm^{-1}) correspond to the amide I, II, and III bonds of gelatin. Similar peaks were reported in previous studies for gelatin [43–45]. Furthermore, the peaks that appeared in the range of 3600–2700 cm^{-1} are associated with Amide A and B, and those detected in the range of 900–400 cm^{-1} corresponded to Amide IV, V, and VI (Fig. 1a) [46].

In the ATR-FTIR results (Fig. 1b), of the cross-linked sodium G-SA hydrogels, the characteristics band observed at around 920 cm^{-1} are related to C–H group [47]. The bands around 1025 cm^{-1} are the C–O–C bonds as identified in sodium alginate as well [48]. Furthermore, the peak at about 1415–1460 cm^{-1} is attributed to COO–, which is linked to the alginate hydrogen [49]. The peak at 1526 cm^{-1} is due to the N–H group of amide II and that observed at 1266 cm^{-1} is associated with the N–H group of amide III of gelatin [49, 50]. The peak appeared at 1625 cm^{-1} is the characteristic of $–CONH_2$ group, indicating that the negative group of sodium alginate was probably linked with positive load of gelatin [51–54]. This measurement suggests that intermolecular interactions occur between alginate and gelatin, signifying that the two polymers have molecular compatibility, which can improve the mechanical properties of hydrogels. The band observed in the range of 2800–2900 cm^{-1} is related to the C–H bond, which is characteristic of the polysaccharides (sodium alginate) [47]. The detected broad peak in the region of 3500–3000 cm^{-1} in the FTIR spectra of the gelatin–sodium alginate hydrogels is indicative of O–H bond (the presence of water) [50]. The hydrogels showed spectra consistent with the peaks that appeared in the patterns of sodium alginate and gelatin. Gelatin is amphoteric in nature due to the attendance of carboxylic and amino groups that can provide a net positive charge at acidic pH and thus is capable of forming a complex with anionic polysaccharides (for instance sodium alginate). This is due to the electrostatic interactions, leading to the hydrogel formation.

Rheology

For assessing the mechanical tolerance of the hydrogels with the external forces, amplitude sweep tests were carried out. The G' and G'' of the hydrogels were measured as a function of shear stress where the angular frequency was constant at 1 Hz (Fig. 2a, c, and e). As indicated in these figures, in all hydrogels, the G' remained larger than G'' until the two curves intersected at a certain shear stress. This shows the hydrogels' elastic nature. Afterward, the G'' values became greater than G' values, signifying fractional hydrogel network breaking. The points that G' and G'' met each other (yield stress (σ)) [55], were 819.73, 260.7, and 227.61 Pa for G1-SA9, G3-SA7, and G5-SA5, respectively. Furthermore, the G' values at the yield stress of G1-SA9, G3-SA7, and G5-SA5 were 2655.1, 1246.4, and 1089.5 Pa, correspondingly. The results obtained here indicate that all hydrogels were mechanically stable, with the highest tolerance of mechanical force for G1-SA9. The G3-SA7 and G5-SA5 hydrogels had almost comparable properties. Furthermore, by decreasing the SA content, both yield stress and storage modulus (G') were decreased. This means that the gels with lower SA are less stiff and undergo plastic deformation at low applied forces.

Furthermore, Fig. 2b, d, and f designates higher G' than G'' values for all hydrogels, meaning that all the hydrogels were in solid-state with good elasticity. Moreover, Fig. 2b

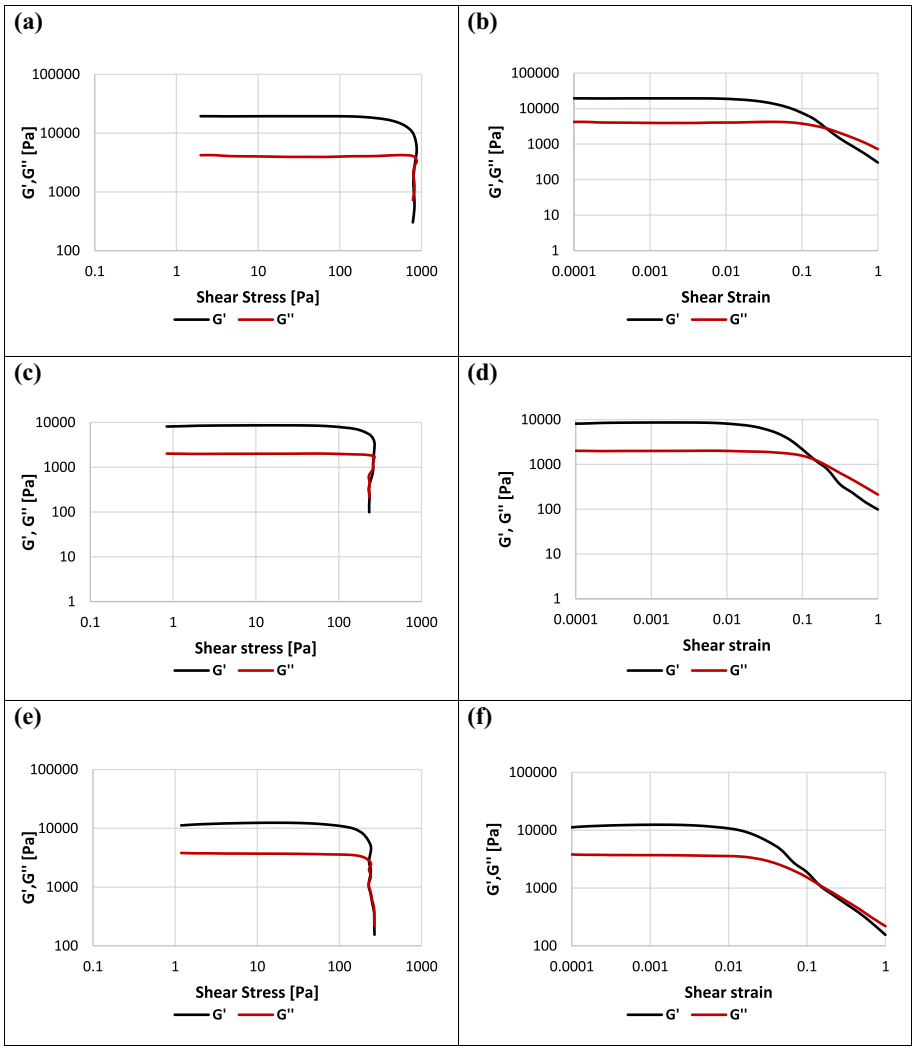

Fig. 2 Rheological characterization of hydrogels. Variations of G' and G'' with different shear stress and strain. **a**, **b** G1-SA9; **c**, **d** G3-SA7; and **e**, **f** G5-SA5

indicates higher G' and G'' values for the G1-SA9 hydrogel, implying that the hydrogel was more solid-like with superior elasticity in comparison with other hydrogel formulations. This was obvious as this hydrogel was very stiff and the preparation and handling were difficult, particularly when the cells were added for biological analyses. The rheological properties of the G1-SA9, G3-SA7, and G5-SA5 hydrogels were only independent of the applied strains up to critical strain levels of 2.15%, 1.47%, and 1.47%, respectively (Fig. 2b, d, and f). Beyond these strain levels, the G' declined and became lower than G''. This is indicative that $<2.15\%$ strain for G1-SA9 and $<1.47\%$ strain for G3-SA7 and G5-SA5, the structure of these hydrogels was undamaged and the hydrogels behaved solid-like, and as the $G' > G''$, the samples were highly structured. However, at the strain level above these critical points, the internal network structure of the hydrogels was disrupted, and they became more fluid-like.

To understand the viscoelastic property of hydrogels, a frequency sweep test was conducted at a constant shear strain of 0.1% and at a constant temperature

of 25 °C. The variations of G' and G'' with oscillatory frequency for the three synthesized hydrogels (G1-SA9, G3-SA7, and G5-SA5) are shown in Fig. 3. The values of G' and G'' in all samples increased when the frequency was amplified (running approximately parallel), and the G' values were always higher than G'' values. Therefore, the dumping factors [56] calculated for the three samples were always less than 1 ($DF = G''/G' < 1$). This means that the internal network structure was formed in all hydrogels across the frequency range, after cross-linking by $CaCl_2$, and the hydrogels had solid-like viscoelastic nature and stability against the applied external force. The G1-SA9 hydrogel was more stable due to greater G' values.

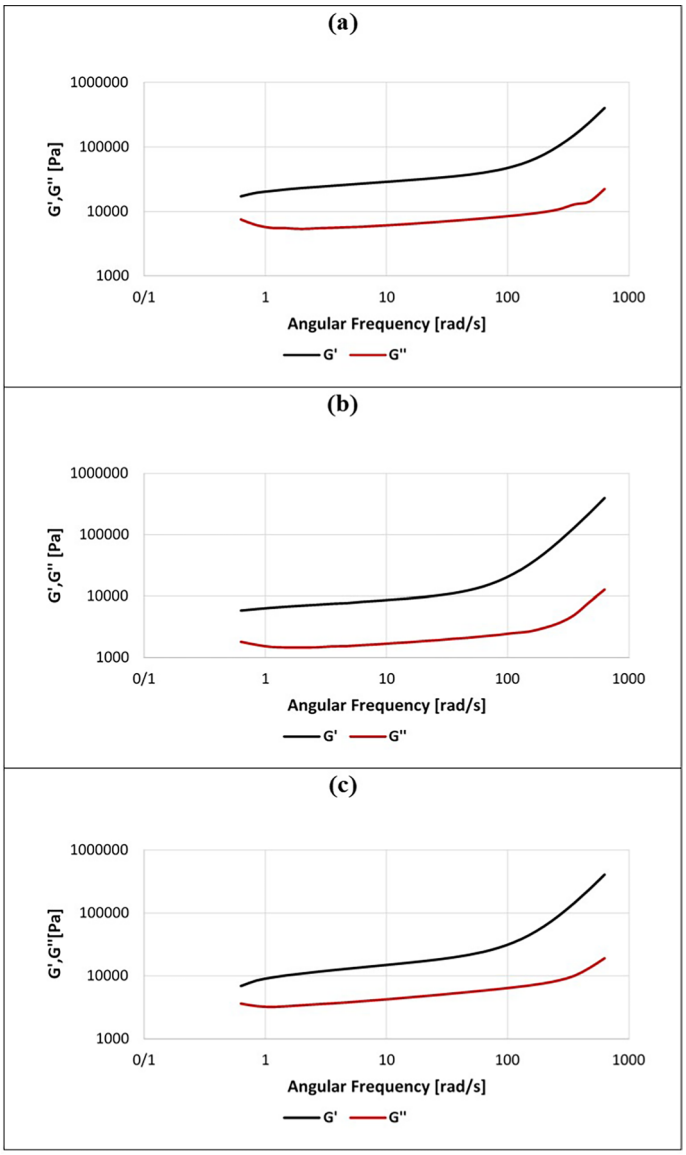

Fig. 3 Rheological characterization of hydrogels. Variations of G' and G'' with different angular frequency: **a** G1-SA9, **b** G3-SA7, and **c** G5-SA5

Surface morphology with and without cells

The SEM images in Fig. 4 demonstrate the surface morphological characteristics of the three hydrogels without cells. As shown in this figure, the surface roughness and topography differ in the three hydrogels, meaning that their compositions influenced the surface and structural properties. It appeared that by increasing the gelatin content in the hydrogels, the surface roughness decreased. The hydrogel with higher content of sodium alginate revealed wrinkled surface, possibly due to strong crosslinking of sodium alginate molecules. Furthermore, SEM images of the hydrogels loaded with U87 (Fig. 5) and C6 (Fig. 6) cells (the glioblastoma cell lines) showed that the cells were well trapped in the hydrogels and their morphology was preserved. Meanwhile, cell aggregation and spheroid formation were also observed. Hence, the results confirmed that the prepared

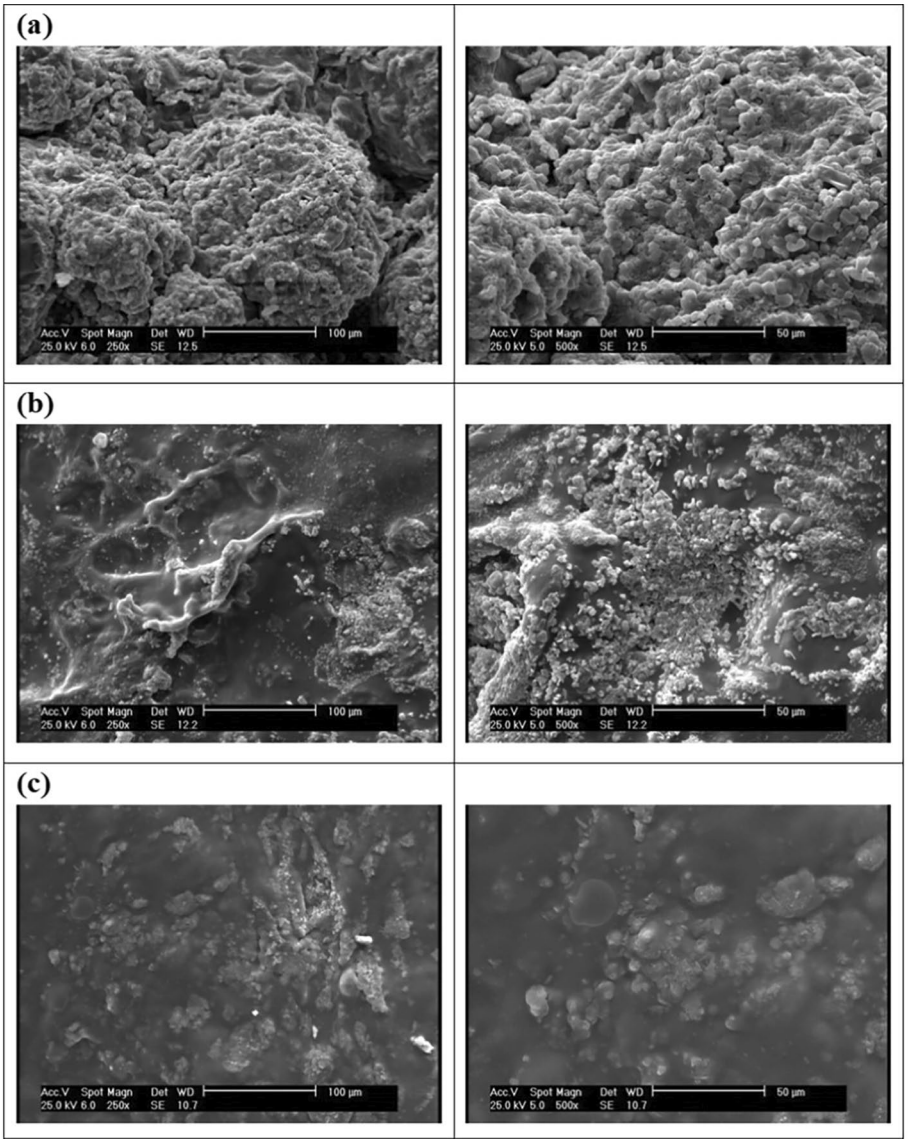

Fig. 4 Hydrogel structures (immediately after preparation and without cells) observed by SEM: **a** G1-SA9, **b** G3-SA7, and **c** G5-SA5 (scale bars: 100, 50 µm)

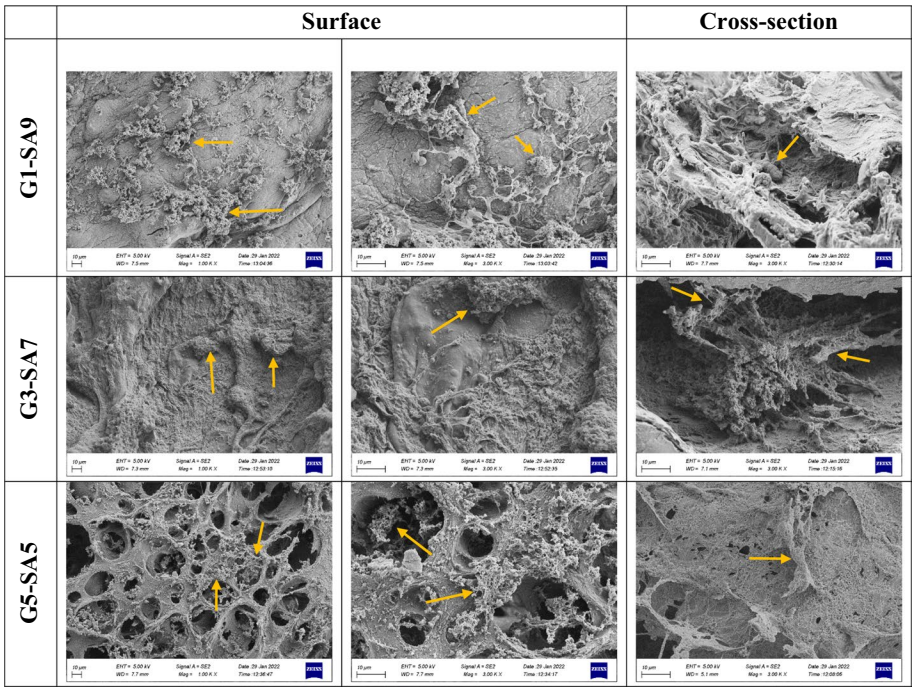

Fig. 5 U87 cells on and inside hydrogels at day 7 observed by SEM. Yellow arrows indicate the cells (scale bar: 10 µm)

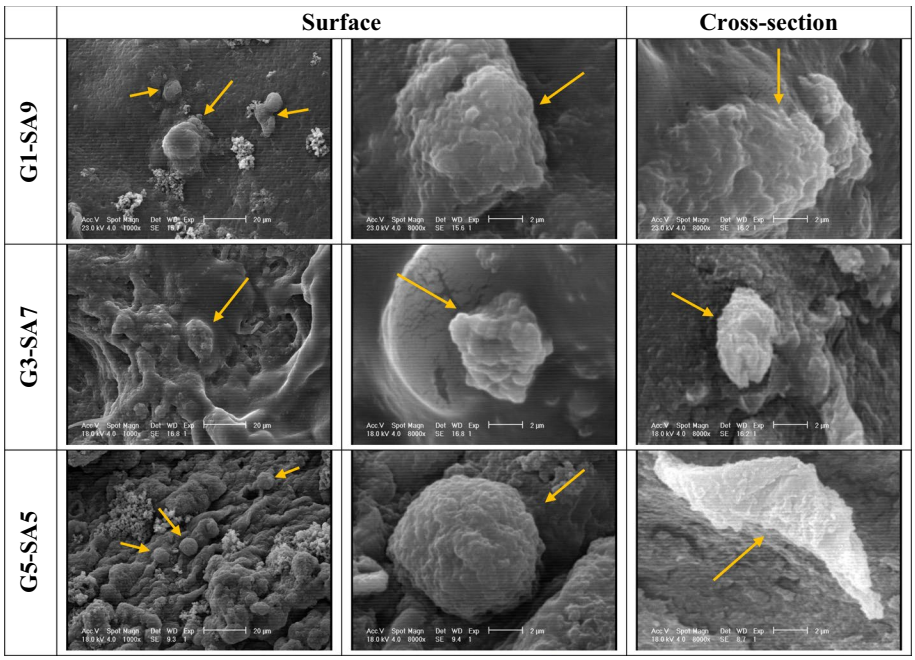

Fig. 6 C6 Cells on and inside hydrogels at day 3 observed by SEM. Yellow arrows indicate the cells (scale bars: 20, 2 µm)

hydrogels not only make possible cell attachment, but also cell spreading, proliferation, and aggregation.

It should be pointed out that both gelatin and sodium alginate are biodegradable polymers, and their hydrogels degrade after a while in aqueous solutions. Several micro-pores were observed in the SEM images (Figs. 5 and 6), probably due to polymer degradation, particularly gelatin. It can be seen that as the gelatin content increased the structure became more porous.

Hydrogel cytotoxicity

The viability of GBM cell lines (C6 and U87) grown in different hydrogel compositions was assessed using a resazurin-based assay at 3 and 7 days. The results displayed that culture of both cell lines in the G5-SA5 composition can induce remarkable proliferation of tumor cells after 7 days. No significant difference was observed at day 3 of the culture (Fig. 7). Thus, the G5-SA5 formula represents a better scaffold structure for cell growth.

Morphology of glioblastoma cells in 3D culture

The morphology of the glioblastoma cell lines (U87 and C6) in the optimal hydrogel scaffold (G5-SA5) was examined on day 7 by conventional histology techniques and confocal microscopy imaging. As shown in Fig. 8a, two cell lines adhered to the scaffolds and grew along the skeleton. Tumor cells cultured in hydrogel scaffolds (Fig. 8a) showed both types of cells proliferated and were morphologically similar to glioblastoma cells in original tumor tissues. The morphology of cancer cell lines in 2D culture are often different from 3D culture. In 2D culture glioblastoma cells were fusiform, flat and epithelioid, while in 3D culture they grow as small, round or ovoid cells [57, 58]. Furthermore, cells were observed in the scaffold after 7 days, stained with phalloidin, and imaged by confocal microscopy. Phalloidin is used for staining actin filaments (actin is the fundamental cytoskeletal molecule). Actin can be stained in living and fixed cells to determine and follow the structure and function of the cytoskeleton. Here, the aim of the phalloidin staining was to confirm and visualize whether the living cells can aggregate and form spheroids. Regarding cell viability, the cells within the hydrogel were alive (stained green) and loaded successfully (Fig. 8b). Similar to SEM images, GBM cell aggregation and spheroid formation were observed in the 3D culture of both cell lines.

Effect of CD73 inhibitor on tumor cell proliferation in the three-dimensional culture

Figure 9a shows the chemical structure of CD73 inhibitor (APCP). The effect of APCP on the viability of C6 and U87 cells was assessed using resazurin-based assays. As shown in Fig. 9b, APCP led to a significant decrease in viability in both GBM cell lines at doses of 50, 100 and 200 μg/ml after 24 h and 48 h compared to the control group. In addition, a dose-dependent effect of the CD73 inhibitor on the proliferation of both cell lines was shown. However, this effect appeared to be saturated at higher concentrations. The dose-dependent effect of the CD73 inhibitor was more pronounced after 24 h than after 48 h. The IC50 values for 24 and 48 h for C6 were 59 and 158 μg/ml, respectively, and the IC50 values after 24 and 48 h for U87 were 70 and 66 μg/ml, respectively. For this reason, we chose a concentration of 100 for the gene expression assay.

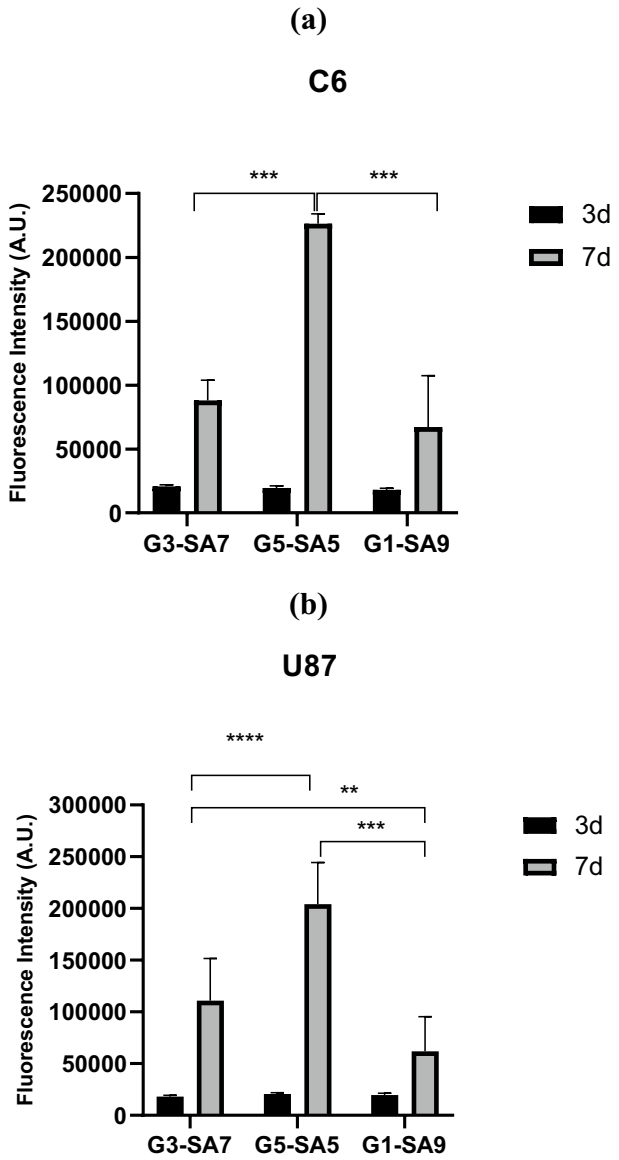

Fig. 7 Cell viability and proliferation analysis of **a** C6, and **b** U87 tumor cell lines cultured in three hydrogel compositions after 3 and 7 days. Bars indicate mean ± SEM. $N = 3$ replicates per condition. $^{**}P < 0.01$, $^{***}P < 0.001$, and $^{****}P < 0.0001$

Effects of CD73 inhibitor treatment on gene expression in 3D model

To assess the effect of CD73 inhibitor on tumor angiogenesis and matrix degradation, the gene expression of VEGF-A, HIF-1α, and MMP9 were quantified in the optimal hydrogel (G5-SA5, Fig. 10) when the cells were exposed to the optimum dose of APCP (100 μg/ml). As can be seen in Fig. 10, treatment with APCP in both glioblastoma cell lines (C6 and U87) considerably decreased the levels of VEGF-A and HIF-1α RNAs compared with the drug solvent-treated cells (control group). MMP9 expression was highly down-regulated in the U87-treated cell lines ($^{*}P < 0.05$). In the C6 cell line, MMP9 expression declined in comparison with the control group however, the differences were not statistically significant.

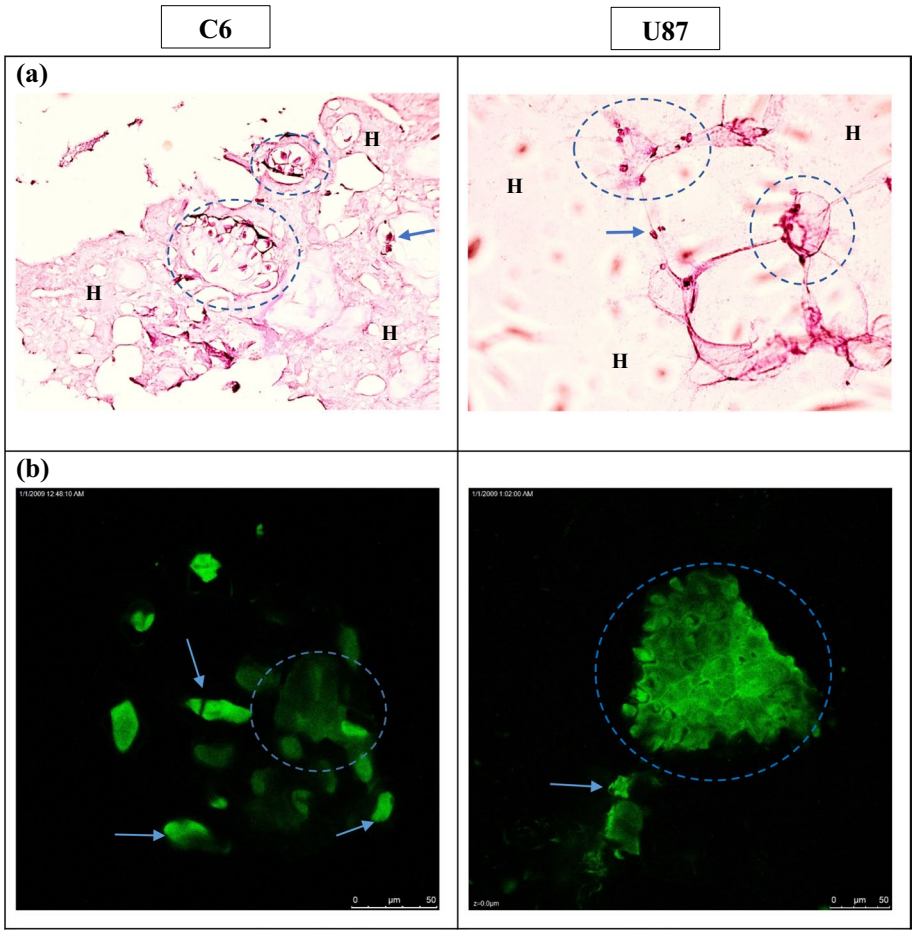

Fig. 8 Morphology of glioblastoma cells. **a** Paraffin-embedded cross-section and H&E staining of the glioblastoma cell lines in the three-dimensional culture (magnification: ×200), (dashed circle: cell aggregate, arrow: single cell, H: hydrogel). **b** Confocal microscopy of tumor cells cultured in hydrogel environments (scale bar: 50 µm) (dashed circle: cell aggregate, arrow: single cell)

Discussion

It is well documented that the tissue microenvironment is important for the angiogenic and metastatic process of tumorigenesis [59]. In their natural 3D environment, malignant cells interact with a variety of cells, including immune and stromal cells, and numerous factors such as cytokines, adenosine, and proteolytic proteins, making this complexity difficult to reproduce in 2D in vitro experiments. 2D cultures have numerous limitations, including disruption of interactions between the cellular and extracellular environments, alteration of cell morphology, polarity, and division method [24, 60]. This complexity has led to the development of various models that can mimic in vivo conditions well, such as 3D culture. Optimizing culture conditions improves our knowledge of tumor biology and facilitates the study of biomarkers and new targeted therapies [61]. In this study, we investigated the growth, viability, and sensitivity of glioblastoma cells in a hydrogel-based 3D culture system.

Three different formulations of gelatin–sodium alginate hydrogels were prepared here. These natural polymers were chosen because sodium alginate is a highly hydrophilic

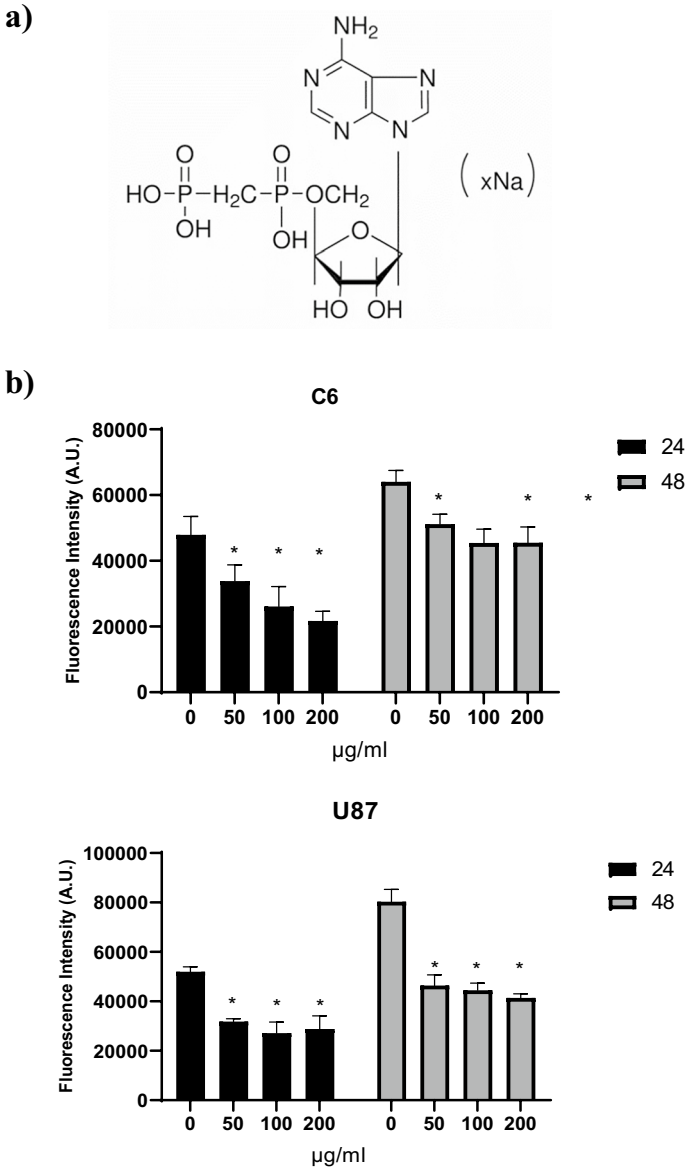

Fig. 9 Effect of CD73 inhibitor on tumor cell proliferation. **a** Structure of APCP (CD73 inhibitor). **b** Proliferation rate of tumor cell line exposed to APCP in hydrogel scaffold after 24 and 48 h. Bars indicate mean ± SEM. $N = 3$ replicates per condition. $^{*}P < 0.05$ compared with control (concentration zero) group

polysaccharide that, due to its loose structure, has abundant hydroxyl and carboxyl groups with free volume between the chains [62, 63]. Furthermore, gelatin is a natural protein that comprises free carboxyl and amino groups on its flexible backbone, and transports positive charges in aqueous solutions. It is expected that promising performance of G-SA hydrogels could be gained due to the charge type, presence of hydrophilic groups, and chain stiffness between these two polymers. In all hydrogels developed here, G and SA could form a cation–anion complex which led to hydrogel formation, and the cells could adhere and aggregate within the hydrogel structures. Furthermore, the hydrogels formed a good internal network structure after cross-linking by $CaCl_2$ and had solid-like viscoelastic nature and stability against the applied external force. However, it

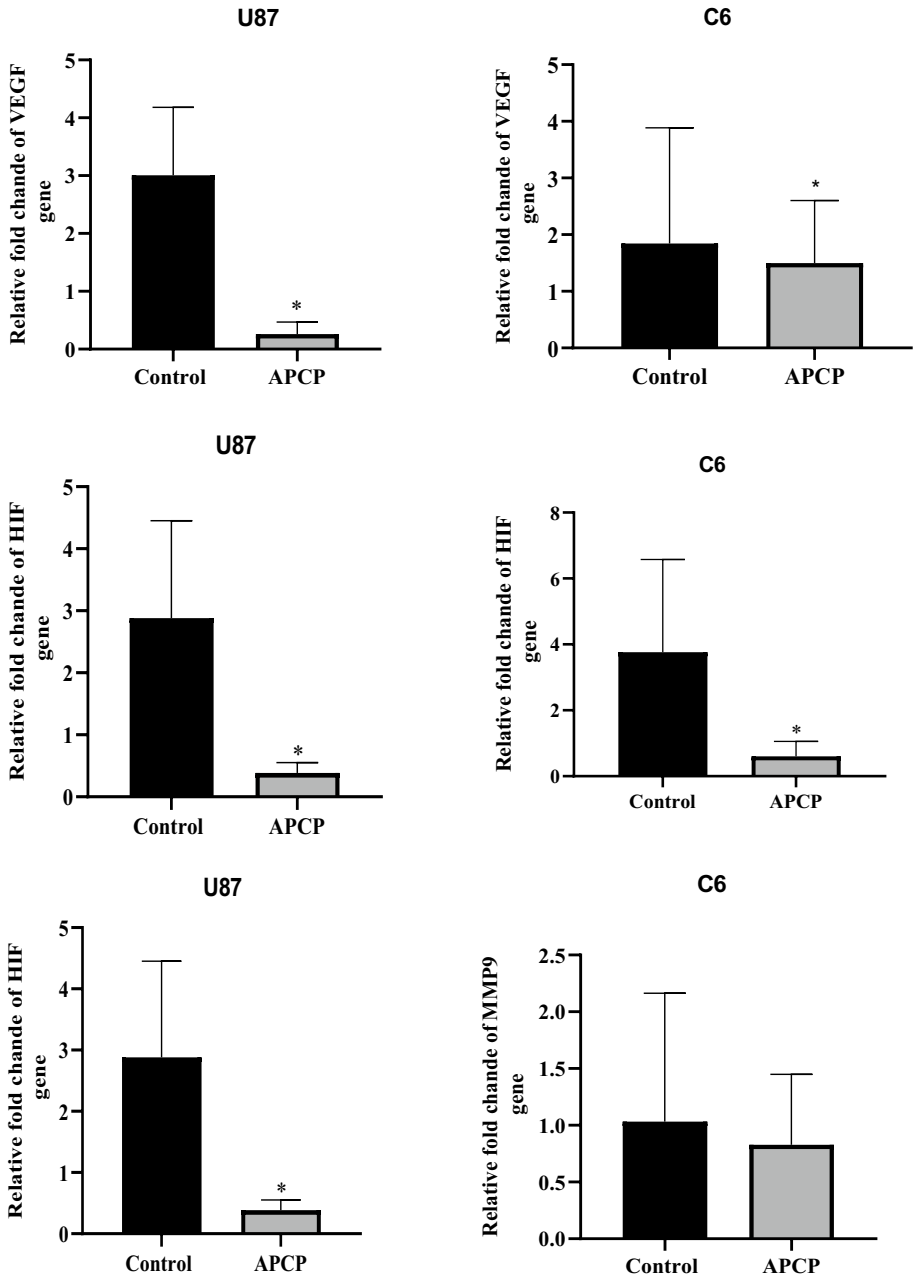

Fig. 10 Relative expression of VEGF-A, HIF-1α, and MMP9 in the 3D hydrogel-based culture model. B2m and GAPDH were regarded as the internal control. Data are represented as the mean ± SEM from 4 samples and were evaluated using a student's *t*-test. **P* < 0.05 in comparison to the control group

should be pointed out that the G1-SA9 hydrogel was very stiff and the preparation and handling were difficult, particularly when the cells were added. It has been indicated that the rheological parameters quantitatively depend upon the ratio of these components in the hydrogel complexes [53]. To select the optimum G-SA hydrogel among the different formulations to be used as the 3D culture system, a preliminary comparative assay on cytocompatibility was performed and finally, the hydrogel with 5w% gelatin and 5w% sodium alginate was chosen because a higher proliferation rate was observed meaning

that this hydrogel provided the superior environment for GBM cells. Gelatin and sodium alginate were previously used as 3D in vitro model systems to induce the formation of breast cancer cell spheroid through bioprinting [29, 30]. The authors in both studies found that the bioprinted heterogeneous model could result in high rate of viability and self-assembly of breast cancer cells to form multicellular tumor spheroids with the cancer-associated fibroblast cells migration and interaction. The hydrogel composition was 3 w/v% alginate and 7 w/v% gelatin. In another study [64], optimized sodium alginate-gelatin hydrogels were printed along with non-small cell lung cancer (NSCLC) patient-derived xenograft (PDX) cells and lung cancer-associated fibroblasts. The hydrogels with 3.25% and 3.5% (w/v) SA and 4% (w/v) G revealed better printability, higher cell viability, and spheroid formation. In addition, several studies developed 3D in vitro model or drug delivery systems for glioblastoma using hydrogels. For example, Fan et al. designed a novel 3D GBM (U87) cell culture model based on microwells made up of poly(ethylene glycol) dimethyl acrylate (PEGDA) hydrogel, which is simple and low-cost. The authors used the photolithography technique to make the 3D micropatterning system in order to control the shape, size, and thickness of the GBM cell spheroids [65]. In another study, different variants of pectin-based hydrogels were developed by change of the pectin concentration and the quantity of free carboxyl groups for anti-glioma therapy [66]. The biological assays on C6 and U87 glioblastoma cells reveled the anti-glioma activity of the developed hydrogels as they decreased cell proliferation and modulated migration, but supported the high neural cell viability.

Animal and cellular studies have already shown that CD73 is a promising target for the treatment of glioblastoma because it is related to tumor growth, angiogenesis, metastasis, escape from immunesurveillance, and chemoresistance [9, 67]. It should be noted that there is no assessment of the effect of CD73 inhibitor on animal and human GBM cell lines in the three-dimensional gelatin–sodium alginate hydrogel culture model. A significant anti-proliferative effect was observed after 48 and 72 h of incubation with the CD73 inhibitor (APCP) tested in the 3D culture model (Fig. 9). Jiglaire et al. fabricated an ex vivo hyaluronic acid-rich hydrogel 3D culture system for U87 glioblastoma cell lines and primary cell cultures of human glioblastomas and then assessed it in comparison with 2D culture conditions. This study showed that 3D hydrogel maintained cancer growth behavior and provide an evaluation of glioblastoma drug sensitivity [68]. Mirani et al. used 3D bioprinted alginate gelatin methacryloyl meshes to enable sustained release of all-trans-retinoic acid (ATRA) for targeted treatment of GBM cells [69]. Dai et al. used porous gelatin/alginate/fibrinogen hydrogel as a 3D bioprinted glioma stem cell model and found that glioma stem cells were more resistant to temozolomide (TMZ) in a 3D tumor model than in a 2D monolayer model [28].

It is well known that angiogenesis and invasion are important processes for tumor progression, growth, and metastasis. Angiogenesis plays a critical role in cancer growth because solid tumors require a blood supply [70]. In our 3D model, APCP treatment resulted in decreased expression of tumor-associated genes related to prevascularization (HIF-1α and VEGF-A) and invasion (MMP9) (Fig. 10). The 3D models of ovary [71], breast cancer [72], glioblastoma [73], and osteosarcoma [74] models showed upregulation of MMPs, HIF-1α, and VEGF-A. Dragoj et al. established alginate fibers for a long-term (28 days) 3D model of U87 cells for temozolomide sensitivity testing and showed

that TMZ treatment reduced cell viability but upregulated chemotherapy resistance-related genes (MGMT and ABCB1) expression [75]. In another study, docetaxel treatment of non-small cell lung cancer cells in a 3D tumor model of alginate scaffolds resulted in diminished Bcl-2 RNA expression versus 2D cultures [76]. 3D culture conditions with appropriate ECM-like body environments appear to bridge the gap between 2D cultures and in vivo models and provide predictions of therapeutic outcomes.

Conclusively, our study demonstrated that the 3D culture model preserves the growth function of glioblastoma. This seems to be a promising method for the massive trials of the anti-cancer compounds, probably in combination with other therapies. Furthermore, a 3D culture system can be employed to predict drug efficacy and develop a personalized medicine approach. This study was a preliminary research on the effectiveness of CD73 inhibitor on glioblastoma cells in a 3D culture model. In the future, it would be interesting to analyze more molecular basis and pathway signaling in this model.

Conclusions

In the present study, different formulations of 3D gelatin–sodium alginate hydrogels were synthesized. We demonstrated that the optimized 3D G-SA hydrogel system can be utilized to provide in vitro tumor culture spheroids. The hydrogel containing 5w% gelatin and 5w% sodium alginate, was selected for its cytocompatibility and rheological behavior. Furthermore, CD73 inhibitor-treated GBM cells significantly decreased the proliferation rate and the expressions of VEGF and HIF1-α within the optimal hydrogel.

Materials and methods

Materials

CD73 inhibitor adenosine 5′-(α,β-methylene) diphosphate (APCP, C11H17N5O9P2, Mw: 425.23, 50 mg/ml solubility in water), and trypsin/EDTA were purchased from Sigma. Dulbecco's Modified Eagle's Medium (DMEM), fetal bovine serum (FBS), penicillin, and streptomycin were purchased from Gibco, Grand Island, USA. Sodium alginate (SA) and Gelatin (G) were provided from Merck, Germany. Phalloidin fluorescent stain was purchased from Thermo Fisher Scientific, Germany.

Hydrogel synthesis

The SA and G powders were placed under UV light for 45 min, and the normal saline solution was autoclaved and immediately transferred under the laminar flow bench to prepare the hydrogels. Gelatin was dissolved in saline solution at 40–50 °C using a magnetic stirrer. When the gelatin was completely dissolved and a uniform solution was prepared, the heating was stopped and SA powder was gradually added and mixed into the gelatin solution. Calcium chloride ($CaCl_2$, 3 M in distilled water) as a cross-linker was added dropwise to the gelatin–alginate mixture to form a stable hydrogel structure (50 µl of 3 M $CaCl_2$ in 1000 µl hydrogel (5 v/v%), equivalent to 16.65 mg/ml). This was done when the hydrogels with or without cells were added into the wells. The whole process was conducted under a laminar flow bench (Fig. 11a). Three uniform composite solutions were prepared based on Table 1 and used for further analyses. These composite hydrogels are illustrated in Fig. 11b.

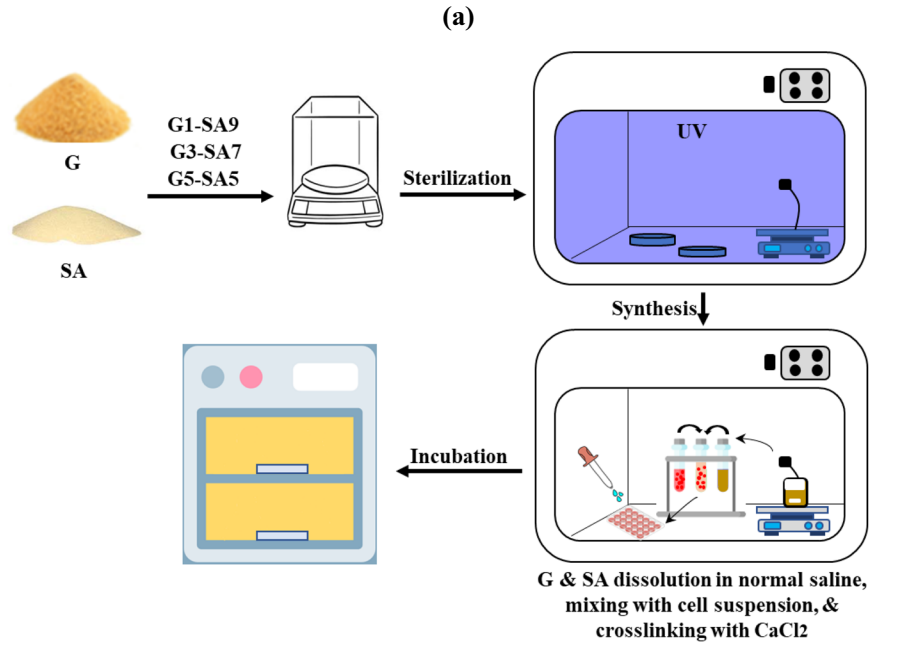

Fig. 11 **a** Schematic of hydrogel synthesis and 3D cell culture processes, and **b** synthesized hydrogels after crosslinking

Table 1 Hydrogel formulations used

No.	Hydrogel name	Hydrogel composition (w/v %) in the normal saline solution		Crosslinker (M)
		SA	G	$CaCl_2$
1	G1-SA9	9	1	3
2	G3-SA7	7	3	
3	G5-SA5	5	5	

Hydrogel characterization

Rheology measurements

Rheological measurements were carried out using a rheometer (Anton Paar, MCR 502). Amplitude sweeps were performed on each set of hydrogels using a two-plate system with parallel plate geometry (25 mm diameter). Three samples were used for each category measurements. The angular frequency was kept constant at 10 radians/s, and the

amplitude excursion angle was varied from 0.1 to 100° excursion. The temperature was kept constant at 37 °C. Each sample was tested with a 2-mm gap between the plates. The storage modulus (G'), loss modulus (G''), and shear stress were all recorded for hydrogel evaluations.

Fourier transform infrared spectroscopy (FTIR)

The structural elucidation and functional groups of the raw powder and freeze–dried hydrogels were identified using NEXUS FT-IR (FTIR and attenuated total reflection (ATR)-FTIR, respectively). The spectra were recorded between 400 and 4000 cm^{-1} at a resolution of 1 cm^{-1}. To do this, the prepared hydrogels were first frozen at − 20 ℃ for 24 h and then freeze–dried for 8 h.

Scanning electron microscopy (SEM)

To analyze the surface morphology of hydrogels by SEM, the samples were first frozen at − 20 °C for 24 h and then freeze–dried for 8 h. The SEM images were taken at an accelerating voltage of 25 kV by Secondary Electron (SE) mode. Prior to imaging, the hydrogels were gold-coated and then examined with MIRA3 FE-SEM (Philips XL30, Netherlands).

Cell line and cell culture

Rat C6 and human U87 glioblastoma cell lines were bought from the National Cell Bank of Iran (Pasteur Institute of Iran, Tehran, Iran). U87 is a glioblastoma, astrocytoma cell line derived from human malignant gliomas [77] and C6 cell line was developed in adult Wistar-Furth rats, after the rats were repetitively exposed to *N*-nitroso-*N*-methylurea exhibited the same histological features as human GBM [78]. The C6 cells were grown in Dulbecco's Modified Eagle's Medium Nutrient Mixture F12 Ham, and the U87 cell line was grown in high glucose Dulbecco's Modified Eagle's Medium containing 10% of fetal bovine serum (FBS), 100 units/ml of penicillin, and 100 µg/ml of streptomycin at 37 °C in a humidified atmosphere of 95% and 5% CO_2 unless otherwise indicated. The passages were performed twice a week after reaching 80–90% confluency using 0.25% trypsin/EDTA.

Three-dimensional hydrogel culture system

To culture C6 and U87 cells in 3D hydrogels, first, the hydrogels were synthesized under sterilized conditions. Then they were gently mixed with the medium containing cells. 1000 µl of the hydrogel medium having 5×10^5 cells was added to each well of the 48-well culture plate. Subsequently, 100 µl of $CaCl_2$ (3M) was inserted to cross-link the hydrogels. Finally, 1000 µl of complete medium was added to the cross-linked hydrogels. The medium was replaced every day with a fresh medium.

Evaluation of cell spheroid formation

H&E staining

Cell-loaded hydrogel samples were fixed in 10% neutral buffered formaldehyde in PBS (formalin solution), dehydrated in 50 v%, 70 v%, 95 v%, and 100 v% ethanol, cleared in xylene, and embedded in paraffin blocks. Paraffin sections (5 µm in thickness) were cut with a microtome and stained for histology with hematoxylin and eosin (H&E). Images

were captured with a microscope-mounted digital camera (Olympus BX-51, Tokyo, Japan).

Confocal microscopy

The cell-loaded hydrogels were first fixed with 4% paraformaldehyde at 4 °C for 15 min. Then, paraformaldehyde was withdrawn and the hydrogels were washed with PBS. To permeable the cells, Triton 0.1% was used for 15 min, and bovine serum albumin (BSA) 2% was added for blocking (60 min). In the end, phalloidin (1.3 μM) was employed to stain the cells within the hydrogels for 1h, and washing was done with PBS several times to remove excessive phalloidin molecules. The images were taken with confocal microscopy (Leica DMi6000B CS TCS SP5).

Scanning electron microscopy

The cell morphology on/inside the hydrogel scaffolds after 3 and 7 days was analyzed by SEM (ZEISS sigma300). In brief, after 3 and 7 days of culture, samples were fixed for 1 h in a solution containing 2.5% (v/v) glutaraldehyde (Sigma). Next, samples were incubated for 10 min in a series of dilute ethanol concentrations of 30 v% to 99.8 v%. Afterward, the samples were frozen for 24h in −80 °C and freeze–dried for 8 h. Then, the samples were coated with gold sputtered before SEM examination.

Cell proliferation

Cell proliferation was assessed using a resazurin-based membrane permeable solution. This solution produces resorufin, a red highly fluorescent compound when reduced. The conversion rate corresponds to the metabolic activity rate of the cells and can be used to assess cell proliferation as described by Czekanska [79]. To assess the cytocompatibility of the three synthetic hydrogels, the C6 and U87 cell lines were seeded into the hydrogels at a density of 5×10^5 cells/well in 24-well plates and cell proliferation was assessed after two times (3 and 7 days). The optimal hydrogel formulation was identified primarily based on the cell growth obtained.

To assess drug effects, both C6 and U87 cell lines were seeded into the optimal hydrogels at a density of 5×10^5 cells per well in 24-well plates. After culturing the cells overnight, their medium was replaced with fresh medium containing different concentrations of APCP (0, 50, 100, and 200 μg/ml). Cell proliferation was determined after two times (24 and 48 h). First, 100 μl of reagent was added to each well containing 900 μl of cell culture medium and incubated for 3 h at 37 °C in a cell culture incubator protected from direct light. Then, resorufin fluorescence was determined using an Infinite M Plex multimode plate reader (Synergy H1 Hybrid Multi-Mode Microplate Reader, BioTek, USA) at excitation and emission wavelengths of 560 and 590 nm, respectively. Results were presented as the mean ± standard error of relative fluorescence units. All samples were run 3 times.

RNA extraction and real-time PCR

The C6 and U87 cells were seeded into the optimal hydrogel at a density of 5×10^5 cells/well of a 24-well plate. After 24 h, their media were changed with fresh media containing 100 μg/ml APCP (optimum dose). The RNA of the cells in the hydrogels was extracted

Table 2 Primers used in qPCR for mRNAs in Wistar rats

Sequence	Name	Size (bp)
B2M	F: 5′-GCTTGCCATTCAGAAAACTCC-3′ R: 5′-GGAAGTTGGGCTTCCCATTCT-3′	74
VEGF-A	F: 5′-TCGGAGAGCAACGTCACTA-3′ R: 5′-TCTTTGGTCTGCATTCACATC-3′	109
HIF-1A	F:5′-GCAGCGATGACACGGAAAC-3′ R: 5′-TTTCAGAGGCAGGTAATGGAGA-3′	129
MMP9	F: 5′-ATCTGTATGGTCGTGGCTCT-3′ R:5′-CATGGGAGGTGCAGTGGGA-3′	119

Table 3 Primers used in qPCR for mRNAs in human

Sequence	Name	Size (bp)
GAPDH	F: 5 GAGTCCACTGGCGTCTTCAC-3′ R: 5′-ATGACGAACATGGGGGCATC-3′	110
VEGF-A	F: 5′-CGCTTACTCTCACCTGCTTCTG-3′ R: 5′-CTGTCATGGGCTGCTTCTTCC-3′	98
HIF-1A	F: 5′-AAGTTCACCTGAGCCTAATAGTCC-3′ R: 5′-GGGTTCTTTGCTTCTGTGTCTTC-3′	123
MMP9	F: 5′-ATCTGTATGGTCGTGGCTCT-3′, R: 5′-CATGGGAGGTGCAGTGGGA-3′	119

after 48h with TRIzol reagent (YT9080, Yekta Tajhiz Azma; Tehran, Iran) according to the manufacturer's protocol. The RNA yields extracted from each sample was 5 µg using Revert Aid™ First Strand cDNA Synthesis Kit (Yekta Tajhiz Azma Co, Iran) which was converted to cDNA. Real-time PCR was carried out through SYBR Green qPCR Master Mix (cat. no. YT2551, Yekta Tajhiz Azma). Oligo 7 software was used for Primer designing and a BLAST search was conducted in order to examine the quality of the primer sequence. The sequence of primers used for RT-PCR amplification is presented in Tables 2 and 3. The Real-Time PCR program has 3 steps; denaturation (95 °C for 15 s), annealing (X[1] °C for 30 s), and extension (72 °C for 30 s). All experiments were performed in triplicate, and relative gene expression levels were analyzed by the 2^{-ddCt} method. The mRNA expression levels were normalized via quantification of B2M (beta2-macroglobulin) in rat samples and GAPDH (glyceraldehyde 3-phosphate dehydrogenase) in human samples, as a reference gene (housekeeping gene).

Statistical analysis

Analysis of variance (ANOVA) and Student's t-test considering a significance level of $P<0.05$ was applied for statistical analyses. All statistical analyses and graph generation were conducted using GraphPad Prism (Version 8). The data were reported as mean ± standard error unless mentioned otherwise.

[1] It is different for every primes.

Acknowledgements
The authors thank the Nervous System Stem Cells Research Center, Semnan University of Medical Sciences, for excellent technical support, collaboration, and provision of facilities for this work. We also thank the Comprehensive Research Laboratory of Semnan University Sciences for its support and services.

Author contributions
Samaneh Arab and Marjan Bahraminasab designed the experiments and supervised the project; Marjan Bahraminasab, Samaneh Arab, Ali Doostmohammadi, Samira Asgharzade, Atefeh Satari, and Farkhonde Hasannejad performed the experiments; Samaneh Arab and Marjan Bahraminasab analyzed data and prepared the figures; Samaneh Arab and Marjan Bahraminasab wrote a first draft of the manuscript. All authors discussed the results of the experiments, edited and approved the final version of the manuscript.

Funding
This study was supported by a grant from Semnan University of Medical Sciences (Grant Number: 1871).

Availability of data and materials
No datasets were generated or analyzed during the current study.

Declarations

Ethics approval and consent to participate
All protocols of this study were approved by Iran National Committee for Ethics in Biomedical Research (ID: IR.SEMUMS.REC.1400.032).

Human and animal rights
No animals/humans were used for studies that are the basis of this research.

Consent for publication
Not applicable.

Competing interests
The authors declare no competing interests.

Received: 15 June 2024 Accepted: 23 November 2024
Published online: 21 December 2024

References

1. Zugazagoitia J, Guedes C, Ponce S, Ferrer I, Molina-Pinelo S, Paz-Ares L. Current challenges in cancer treatment. Clin Ther. 2016;38(7):1551–66.
2. Khamisabadi M, Arab S, Motamedi M, Khansari NE, Moazeni S, Gheflati Z, et al. Listeria monocytogenes activated dendritic cell based vaccine for prevention of experimental tumor in mice. Iran J Immunol. 2008;5(1):36–44.
3. Nabors LB, Portnow J, Ahluwalia M, Baehring J, Brem H, Brem S, et al. Central nervous system cancers, version 3.2020, NCCN clinical practice guidelines in oncology. J Natl Compr Cancer Netw. 2020;18(11):1537–70.
4. McCutcheon IE, Preul MC. Historical perspective on surgery and survival with glioblastoma: how far have we come? World Neurosurg. 2021;149:148–68.
5. Arab S, Ghasemi S, Ghanbari A, Bahraminasab M, Satari A, Mousavi M, et al. Chemopreventive effect of spirulina microalgae on an animal model of glioblastoma via down-regulation of PI3K/AKT/mTOR and up-regulation of miR-34a/miR-125B expression. Phytother Res. 2021;35(11):6452–61.
6. Nooshabadi VT, Arab S. Targeting tumor-derived exosomes expressing CD73: new opportunities in the pathogenesis and treatment of cancer. Curr Mol Med. 2021;21(6):476–83.
7. Arab S, Alizadeh A, Asgharzade S. Tumor-resident adenosine-producing mesenchymal stem cells as a potential target for cancer treatment. Clin Exp Med. 2021;21(2):205–13.
8. Allard BTM, Spring K, Pommey S, Royal I, Stagg J. Anti-CD73 therapy impairs tumor angiogenesis. Int J Cancer. 2014;134(6):1466–73.
9. Azambuja J, Schuh R, Michels L, Iser I, Beckenkamp L, Roliano G, et al. Blockade of CD73 delays glioblastoma growth by modulating the immune environment. Cancer Immunol Immunother. 2020;69(9):1801–12.
10. Tsiampali J, Neumann S, Giesen B, Koch K, Maciaczyk D, Janiak C, et al. Enzymatic activity of CD73 modulates invasion of gliomas via epithelial–mesenchymal transition-like reprogramming. Pharmaceuticals. 2020;13(11):378.
11. Wang J, Matosevic S. NT5E/CD73 as correlative factor of patient survival and natural killer cell infiltration in glioblastoma. J Clin Med. 2019;8(10):1526.
12. Xu S, Shao Q-Q, Sun J-T, Yang N, Xie Q, Wang D-H, et al. Synergy between the ectoenzymes CD39 and CD73 contributes to adenosinergic immunosuppression in human malignant gliomas. Neuro Oncol. 2013;15(9):1160–72.
13. Allard B, Pommey S, Smyth MJ, Stagg J. Targeting CD73 enhances the antitumor activity of anti-PD-1 and anti-CTLA-4 mAbsAnti-CD73 synergizes with Anti-PD-1 and Anti-CTLA-4 mAbs. Clin Cancer Res. 2013;19(20):5626–35.
14. Goswami S, Walle T, Cornish AE, Basu S, Anandhan S, Fernandez I, et al. Immune profiling of human tumors identifies CD73 as a combinatorial target in glioblastoma. Nat Med. 2020;26(1):39–46.
15. Bielenberg DR, Zetter BR. The contribution of angiogenesis to the process of metastasis. Cancer J. 2015;21(4):267–73.
16. Eguchi R, Kawabe J-I, Wakabayashi I. VEGF-independent angiogenic factors: beyond VEGF/VEGFR2 signaling. J Vasc Res. 2022;59(2):78–89.

17. Dobra G, Gyukity-Sebestyén E, Bukva M, Harmati M, Nagy V, Szabó Z, et al. MMP-9 as prognostic marker for brain tumours: a comparative study on serum-derived small extracellular vesicles. Cancers. 2023;15(3):712.
18. Azimian Zavareh V, Rafiee L, Sheikholeslam M, Shariati L, Vaseghi G, Savoji H, et al. Three-dimensional in vitro models: a promising tool to scale-up breast cancer research. ACS Biomater Sci Eng. 2022;8(11):4648–72.
19. Jubelin C, Muñoz-Garcia J, Griscom L, Cochonneau D, Ollivier E, Heymann M-F, et al. Three-dimensional in vitro culture models in oncology research. Cell Biosci. 2022;12(1):1–28.
20. Birgersdotter A, Sandberg R, Ernberg I. Gene expression perturbation in vitro—a growing case for three-dimensional (3D) culture systems. Semin Cancer Biol. 2005;15(5):405–12.
21. Edmondson R, Broglie JJ, Adcock AF, Yang L. Three-dimensional cell culture systems and their applications in drug discovery and cell-based biosensors. Assay Drug Dev Technol. 2014;12(4):207–18.
22. Bédard P, Gauvin S, Ferland K, Caneparo C, Pellerin È, Chabaud S, et al. Innovative human three-dimensional tissue-engineered models as an alternative to animal testing. Bioengineering. 2020;7(3):115.
23. Jensen C, Teng Y. Is it time to start transitioning from 2D to 3D cell culture? Front Mol Biosci. 2020;7:33.
24. Barbosa MA, Xavier CP, Pereira RF, Petrikaitė V, Vasconcelos MH. 3D cell culture models as recapitulators of the tumor microenvironment for the screening of anti-cancer drugs. Cancers. 2021;14(1):190.
25. Łabowska MB, Cierluk K, Jankowska AM, Kulbacka J, Detyna J, Michalak I. A review on the adaption of alginate–gelatin hydrogels for 3D cultures and bioprinting. Materials. 2021;14(4):858.
26. Law AM, de la Fuente LR, Grundy TJ, Fang G, Valdes-Mora F, Gallego-Ortega D. Advancements in 3D cell culture systems for personalizing anti-cancer therapies. Front Oncol. 2021;11: 782766.
27. Monteiro MV, Gaspar VM, Ferreira LP, Mano JF. Hydrogel 3D in vitro tumor models for screening cell aggregation mediated drug response. Biomater Sci. 2020;8(7):1855–64.
28. Dai X, Ma C, Lan Q, Xu T. 3D bioprinted glioma stem cells for brain tumor model and applications of drug susceptibility. Biofabrication. 2016;8(4): 045005.
29. Jiang T, Munguia-Lopez J, Flores-Torres S, Grant J, Vijayakumar S, De Leon-Rodriguez A, et al. Bioprintable alginate/gelatin hydrogel 3D in vitro model systems induce cell spheroid formation. JoVE. 2018;137: e57826.
30. Jiang T, Munguia-Lopez JG, Flores-Torres S, Grant J, Vijayakumar S, Leon-Rodriguez AD, et al. Directing the self-assembly of tumour spheroids by bioprinting cellular heterogeneous models within alginate/gelatin hydrogels. Sci Rep. 2017;7(1):4575.
31. Abasalizadeh F, Moghaddam SV, Alizadeh E, Akbari E, Kashani E, Fazljou SMB, et al. Alginate-based hydrogels as drug delivery vehicles in cancer treatment and their applications in wound dressing and 3D bioprinting. J Biol Eng. 2020;14:1–22.
32. Ge X, Xu X, Cai Q, Xiong H, Xie C, Hong Y, et al. Live mapping of the brain extracellular matrix and remodeling in neurological disorders. Small Methods. 2024;8(1):2301117.
33. Bahraminasab M, Janmohammadi M, Arab S, Talebi A, Nooshabadi VT, Koohsarian P, et al. Bone scaffolds: an incorporation of biomaterials, cells, and biofactors. ACS Biomater Sci Eng. 2021;7(12):5397–431.
34. Echave MC, Burgo LS, Pedraz JL, Orive G. Gelatin as biomaterial for tissue engineering. Curr Pharm Design. 2017;23(24):3567–84.
35. Mūnoz Z, Shih H, Lin CC. Gelatin hydrogels formed by orthogonal thiol-norbornene photochemistry for cell encapsulation. Biomater Sci. 2014;2(8):1063–72.
36. Khajavi S, Bahraminasab M, Arab S, Talebi A, Kokhaei P, Abdoos H. Design and synthesis of berberine loaded nano-hydroxyapatite/gelatin scaffold for bone cancer treatment. New J Chem. 2024;48(15):6977–96.
37. Landers R, Hübner U, Schmelzeisen R, Mülhaupt R. Rapid prototyping of scaffolds derived from thermoreversible hydrogels and tailored for applications in tissue engineering. Biomaterials. 2002;23(23):4437–47.
38. Zehnder T, Sarker B, Boccaccini AR, Detsch R. Evaluation of an alginate–gelatine crosslinked hydrogel for bioplotting. Biofabrication. 2015;7(2): 025001.
39. Sarker B, Rompf J, Silva R, Lang N, Detsch R, Kaschta J, et al. Alginate-based hydrogels with improved adhesive properties for cell encapsulation. Int J Biol Macromol. 2015;78:72–8.
40. Pereira R, Tojeira A, Vaz DC, Mendes A, Bártolo P. Preparation and characterization of films based on alginate and aloe vera. Int J Polym Anal Charact. 2011;16(7):449–64.
41. Rao KM, Rao KK, Sudhakar P, Rao KC, Subha M. Synthesis and characterization of biodegradable poly (vinyl caprolactam) grafted on to sodium alginate and its microgels for controlled release studies of an anticancer drug. J Appl Pharm Sci. 2013;3(6):061–9.
42. Febrianastuti S, Fadillah G, Putri ENK, Apriani UW, Wahyuningsih S. Effect of pH $CaCl_2$ solution on graphene oxide encapsulated alginate (GO-AL) for removing methylene blue dyes. IOP Conf Ser Mater Sci Eng. 2019. https://doi.org/10.1088/1757-899X/509/1/012143.
43. Derkach SR, Voron'ko NG, Sokolan NI, Kolotova DS, Kuchina YA. Interactions between gelatin and sodium alginate: UV and FTIR studies. J Dispers Sci Technol. 2019;41(5):690–8.
44. Sohar O. Fourier transform infrared (FTIR) spectroscopic study of extracted gelatin from shaari (*Lithrinus microdon*) skin: effects of extraction conditions. Int Food Res J. 2012;19(3):1167–73.
45. Muyonga J, Cole C, Duodu K. Fourier transform infrared (FTIR) spectroscopic study of acid soluble collagen and gelatin from skins and bones of young and adult Nile perch (*Lates niloticus*). Food Chem. 2004;86(3):325–32.
46. Al-Saidi G, Al-Alawi A, Rahman M, Guizani N. Fourier transform infrared (FTIR) spectroscopic study of extracted gelatin from shaari (*Lithrinus microdon*) skin: effects of extraction conditions. Int Food Res J. 2012;19(3):1167–73.
47. Abbasiliasi S, Shun TJ, Ibrahim TAT, Ismail N, Ariff AB, Mokhtar NK, et al. Use of sodium alginate in the preparation of gelatin-based hard capsule shells and their evaluation in vitro. RSC Adv. 2019;9(28):16147–57.
48. Boateng J, Burgos-Amador R, Okeke O, Pawar H. Composite alginate and gelatin based bio-polymeric wafers containing silver sulfadiazine for wound healing. Int J Biol Macromol. 2015;79:63–71.
49. Wen Y, Yu B, Zhu Z, Yang Z, Shao W. Synthesis of antibacterial gelatin/sodium alginate sponges and their antibacterial activity. Polymers. 2020;12(9):1926.
50. Wu Z, Li Q, Xie S, Shan X, Cai Z. In vitro and in vivo biocompatibility evaluation of a 3D bioprinted gelatin–sodium alginate/rat Schwann-cell scaffold. Mater Sci Eng C. 2020;109: 110530.

51. Devi N, Hazarika D, Deka C, Kakati D. Study of complex coacervation of gelatin A and sodium alginate for microencapsulation of olive oil. J Macromol Sci Part A. 2012;49(11):936–45.
52. Saravanan M, Rao KP. Pectin–gelatin and alginate–gelatin complex coacervation for controlled drug delivery: influence of anionic polysaccharides and drugs being encapsulated on physicochemical properties of microcapsules. Carbohydr Polym. 2010;80(3):808–16.
53. Derkach SR, Kuchina YA, Kolotova DS, Voron'ko NG. Polyelectrolyte polysaccharide–gelatin complexes: rheology and structure. Polymers. 2020;12(2):266.
54. Xiao C, Liu H, Lu Y, Zhang L. Blend films from sodium alginate and gelatin solutions. J Macromol Sci Part A. 2001;38(3):317–28.
55. Guchhait S, Roy S. Efficient peptide based gelators for aromatic organic solvents and vegetable oils: application in phase selective gelation and dye entrapment. J Sol-Gel Sci Technol. 2019;89(3):852–65.
56. Roy A, Roy S, Pradhan A, Maiti Choudhury S, Ranjan NR. Gel-emulsion properties of nontoxic nicotinic acid-derived glucose sensor. Ind Eng Chem Res. 2018;57(8):2847–55.
57. Lv D, Yu S-C, Ping Y-F, Wu H, Zhao X, Zhang H, et al. A three-dimensional collagen scaffold cell culture system for screening anti-glioma therapeutics. Oncotarget. 2016;7(35):56904.
58. Jia W, Jiang X, Liu W, Wang L, Zhu B, Zhu H, et al. Effects of three-dimensional collagen scaffolds on the expression profiles and biological functions of glioma cells. Int J Oncol. 2018;52(6):1787–800.
59. Baghban R, Roshangar L, Jahanban-Esfahlan R, Seidi K, Ebrahimi-Kalan A, Jaymand M, et al. Tumor microenvironment complexity and therapeutic implications at a glance. Cell Commun Signal. 2020;18:1–19.
60. Di Modugno F, Colosi C, Trono P, Antonacci G, Ruocco G, Nisticò P. 3D models in the new era of immune oncology: focus on T cells, CAF and ECM. J Exp Clin Cancer Res. 2019;38(1):1–14.
61. Kapałczyńska M, Kolenda T, Przybyła W, Zajączkowska M, Teresiak A, Filas V, et al. 2D and 3D cell cultures—a comparison of different types of cancer cell cultures. Arch Med Sci. 2018;14(4):910–9.
62. Ngah WW, Fatinathan S. Adsorption of Cu (II) ions in aqueous solution using chitosan beads, chitosan–GLA beads and chitosan–alginate beads. Chem Eng J. 2008;143(1–3):62–72.
63. Li Y, Jia H, Cheng Q, Pan F, Jiang Z. Sodium alginate–gelatin polyelectrolyte complex membranes with both high water vapor permeance and high permselectivity. J Membr Sci. 2011;375(1–2):304–12.
64. Mondal A, Gebeyehu A, Miranda M, Bahadur D, Patel N, Ramakrishnan S, et al. Characterization and printability of sodium alginate–gelatin hydrogel for bioprinting NSCLC co-culture. Sci Rep. 2019;9(1):1–12.
65. Fan Y, Avci NG, Nguyen DT, Dragomir A, Akay YM, Xu F, et al. Engineering a high-throughput 3-D in vitro glioblastoma model. IEEE J Transl Eng Health Med. 2015;3:1–8.
66. Belousov A, Patlay A, Silantev V, Kovalev VV, Kumeiko V. Preparation of hydrogels based on modified pectins by tuning their properties for anti-glioma therapy. Int J Mol Sci. 2022;24(1):630.
67. Azambuja J, Gelsleichter N, Beckenkamp L, Iser I, Fernandes M, Figueiró F, et al. CD73 downregulation decreases in vitro and in vivo glioblastoma growth. Mol Neurobiol. 2019;56(5):3260–79.
68. Jiglaire CJ, Baeza-Kallee N, Denicolaï E, Barets D, Metellus P, Padovani L, et al. Ex vivo cultures of glioblastoma in three-dimensional hydrogel maintain the original tumor growth behavior and are suitable for preclinical drug and radiation sensitivity screening. Exp Cell Res. 2014;321(2):99–108.
69. Mirani B, Pagan E, Shojaei S, Duchscherer J, Toyota BD, Ghavami S, et al. A 3D bioprinted hydrogel mesh loaded with all-trans retinoic acid for treatment of glioblastoma. Eur J Pharmacol. 2019;854:201–12.
70. Saman H, Raza SS, Uddin S, Rasul K. Inducing angiogenesis, a key step in cancer vascularization, and treatment approaches. Cancers. 2020;12(5):1172.
71. Xu G, Yin F, Wu H, Hu X, Zheng L, Zhao J. In vitro ovarian cancer model based on three-dimensional agarose hydrogel. J Tissue Eng. 2014;5:2041731413520438.
72. Wang Y, Mirza S, Wu S, Zeng J, Shi W, Band H, et al. 3D hydrogel breast cancer models for studying the effects of hypoxia on epithelial to mesenchymal transition. Oncotarget. 2018;9(63):32191.
73. Pedron S, Harley B. Impact of the biophysical features of a 3D gelatin microenvironment on glioblastoma malignancy. J Biomed Mater Res Part A. 2013;101(12):3404–15.
74. Jiang T, Xu G, Chen X, Huang X, Zhao J, Zheng L. Impact of hydrogel elasticity and adherence on osteosarcoma cells and osteoblasts. Adv Healthc Mater. 2019;8(9):1801587.
75. Dragoj M, Stojkovska J, Stanković T, Dinić J, Podolski-Renić A, Obradović B, et al. Development and validation of a long-term 3D glioblastoma cell culture in alginate microfibers as a novel bio-mimicking model system for preclinical drug testing. Brain Sci. 2021;11(8):1025.
76. Godugu C, Patel AR, Desai U, Andey T, Sams A, Singh M. AlgiMatrix™ based 3D cell culture system as an in-vitro tumor model for anticancer studies. PLoS ONE. 2013;8(1): e53708.
77. Schulz JA, Rodgers LT, Kryscio RJ, Hartz A, Bauer B. Characterization and comparison of human glioblastoma models. BMC Cancer. 2022;22(1):1–18.
78. Giakoumettis D, Kritis A, Foroglou N. C6 cell line: the gold standard in glioma research. Hippokratia. 2018;22(3):105.
79. Czekanska EM. Assessment of cell proliferation with resazurin-based fluorescent dye. In: Mammalian cell viability: methods and protocols. Totowa: Humana Press; 2011. p. 27–32.

Publisher's Note